ISET Journal of Earthquake Technology, Paper No. 589, Vol. 61, No. 4, Dec. 2024, pp. 107-120

45th ISET Annual Lecture

INSTABILITY OF MOUNTAIN SLOPES UNDERGOING LONG-TERM EFFECTS OF FAULT ACTION

I. Towhata
Visiting Professor, Kanto Gakuin University
E mail id: towhata.ikuo.ikuo@gmail.com

ABSTRACT

This paper addresses the relationship between earthquake-induced disasters and fault activities. Although the coseismic landslide was one of the important issues in the previous century, the changing life style in this century requires new perspectives. First, case histories are investigated to reveal that many coseismic landslides occur along faults, which are either causative or existing nonactive. Second, this point is discussed more in detail by taking example landslides along several existing faults. In particular, those faults with very long history, which have been active for millions of years or tens of millions years, are studied. Because of the kilometers of accumulated fault dislocation along such a fault, the nearby rock mass has been disrupted mechanically and is prone to erosion. Thus, valleys are formed in mountains and big alluvial fans are formed in the downstream area. This big size of alluvial fan means slope instability in the upstream region that results in the higher risk of flash floods and debris flows. Finally, the discussion is made of two fault-related problems. The first one is the recent experiences in Türkiye in 2023 where fault rupture propagated very fast. This phenomenon is called supershear and produces strong shaking with elongated shaking period towards the end tip of the causative fault. This kind of ground shaking is destructive to structures and is seemingly one of the main cause of major damage as occurred in Türkiye. Another fault-related problem is the tectonic uplift that occurred with a significant extent during the 2024 Noto Peninsula earthquake, Japan, and hindered the operation of harbors during the emergency.

KEYWORDS: fault, slope instability, erosion, supershear, tectonic uplift

INTRODUCTION

The landslides triggered by earthquakes have been, are, and will be one of the very important disaster mechanisms. However, because lifestyle of human is changing with time, the major issues of earthquake-induced landslides are changing with time as well. In the 20th Century, of major concern was the extent of instability in slopes in and near human communities. In this regard, much study was made of the effects of epicentral distance, intensity of ground motion, topography, elevation in mountain relief, slope gradient, local geology, etc. In spite of those efforts, it did not become possible to evaluate the coseismic stability of a particular slope during future earthquakes, obviously because subsurface investigation on geology and hydrogeology was missing due to financial limitation. Nevertheless, it became possible to a certain extent to assess the hazard of coseismic landslides in areas such as 500m×500m grids (Kanagawa Prefectural Government, 1986). Despite using GSI and many other novel technologies in the 21st century, it appears to the author that there is no substantial improvement in the quality of assessment after that stage, because the fundamental problem of the lack of subsurface investigation (shortage of funding) has not been solved.

New issues in the 21st Century arose after the experiences of the 1999 Chi Chi earthquake in Taiwan (moment magnitude Mw = 7.7) and the 2008 Wenchuan earthquake in China (7.9-8.3 in Mw scale) with some more events. Those issues are briefly summarized as

- Natural dams made by a landslide mass and their possible breaching and flooding afterwards,
- Compound effects of earthquake and rainfall on slope instability, and
- Long-term instability of affected slopes after strong earthquakes.

In addition, the author was impressed during the Wenchuan earthquake and the 2005 event in Northern Pakistan of Mw = 7.6 that the existing non-active faults influenced the extent of landslide disasters both

during and after the earthquakes. In this perspective, the present paper describes the relation between faults and slope disasters as observed in recent events.

CONCENTRATION OF COSEISMIC LANDSLIDES IN SHORT DISTANCE FROM FAULTS

The 1897 Assam earthquake of (*M*w = 8.2-8.3) triggered substantial landslides and Oldham (1899) reported in his Figures 1 and 3 that the mountain slopes had considerably lost their vegetation coverage. The 1950 Assam earthquake (*M*w = 8.7) was associated with many coseismic landslides again and the consequent erosion in the affected slopes raised riverbeds during floods in the later period (Kingdon-Ward, 1953). Thus, strong seismic shaking often triggers landslide disasters.

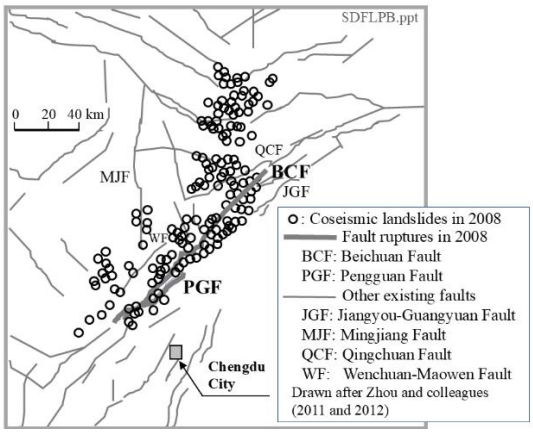

Fig. 1 Location of landslides triggered during and after the 2008 Wenchuan earthquake

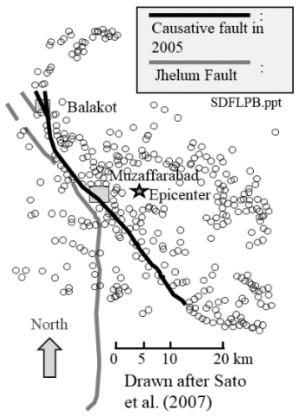

Fig. 2 Location of landslides that occurred during and after the 2005 earthquake in Northern Pakistan

To provide more examples Figures 1 and 2 show the location of landslides triggered by the aforementioned two big earthquakes in China and Pakistan. In the case of China, the affected area is at the eastern edge of the Tibet Plateau that has been geologically pushing against the present China and has mechanically disturbed the slopes at the interface. Consequently, many landslides occurred in 2008 (Figure 3) not only along the causative faults (BCF and PGF in Figure 1) but also in the northern weak areas where the 1933 Diexi earthquake (*M*w = 7.3) created many large landslide dams (Chang, 1938) together with the 2017 Xinmo nonseismic landslide of 3.6 million cubic meters in volume (Meng et al., 2018). These examples imply a close correlation between the long-term tectonic activities with geological rock disturbance and the hazard of coseismic landslides. A similar situation was found after the 2005 earthquake in Northern Pakistan (Figure 2). Figure 4 shows a substantial number of landslides concentrated along the causative fault. Those slides were partly triggered by strong shaking near the causative fault but, to the east of the fault in Figure 2, were partly associated with the disturbed or fractured weak rock mass (Figure 5). Vermilye and Scholz (1998) called this mechanical damage in rock mass “process zone”.

Fig. 3 One of the coseismic landslides triggered by the 2008 Wenchuan earthquake, China

Fig. 4 Coseismic landslides in 2005 in Northern Pakistan, aligned along a fault valley near Balakot

The importance of tectonic disturbance/disruption of rock mass is found in Nepal as well. Being located at the site of collision of two continental plates, slopes in Nepal are often composed of fractured rock. Figure 6 illustrates an example situation in Batua, south of Tansen in Lesser Himalayan Range, Nepal (Hasegawa et al., 2009). There are many faults in this range and the siltstone in this unstable slope has been ground into powder. Thus, many large-scale landslides during the 2015 Gorkha earthquake (Mw = 7.8) and other events are likely the consequences of the tectonic plate-to-plate collision; refer to Regmi et al. (2013).

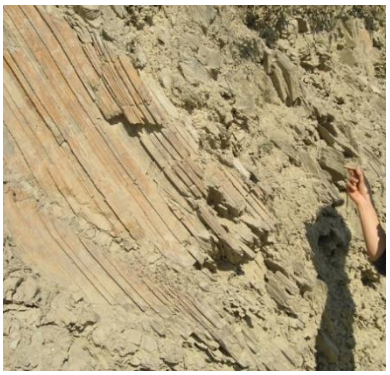

Fig. 5 Fractured rock near Muzaffarabad, Pakistan

Fig. 6 Ground surface covered by powder of crushed siltstone, south of Tansen, Nepal

The 2004 Niigata-Chuetsu earthquake of Mw = 6.6 in Japan triggered many landslides in the Higashiyama Hills in the epicentral region (Figure 7). Being made of synclines and anticlines, this hilly terrain had been prone to landslides, implying the mechanical deterioration of the rock mass. Moreover, this hilly area had about 50% of its area composed of mud stone. It seems that, in the surface of slopes, the low confining stress allowed water absorption of mud stone and resulted in decay of the stone to just mud. This was particularly the case in road embankment made of crushed mud stone (Figure 8). Consequently, many coseismic landslides occurred and the rescue work by ground transportation became impossible.

Fig. 7 One of the landslides in former Yama-koshi Village triggered by the 2004 Nii-gata-Chuetsu earthquake

Fig. 8 Coseismic failure of road embankment in the same area as in Figure 7

SLOPE INSTABILITY ALONG EXISTING NON-SEISMIC FAULTS

This section addresses the slope instability along existing faults that did not rupture during particular recent earthquakes but promoted the slope disasters. This issue was touched upon in Figures 1 and 2 in which concentration of slope instability along existing faults was presented.

Itoigawa-Shizuoka Tectonic Line in Central Japan (Figure 9) is one of the two important tectonic lines of the nation and crosses the Honshu Island. It is interesting that the southern-most segment of this tectonic line near the Pacific Ocean, which is called the Minobu Fault, has several long-term slope instability in its western vicinity; Figure 10. Figure 11 illustrates the unstable slope of Mt. Shichimenzan in Figure 10 that is made of mechanically disturbed materials. A local legend dated AD 1278 mentioned this landslide and this mountain has undergone long-term instability and creep deformation as shown by a pond and depression at the mountain top. Nagai and Nakamura (2000) stated that the local rock mass has been

compressed tectonically in East-West direction and damaged by this stress together with the fault-induced shear produced by the Itoigawa-Shizuoka Tectonic Line. Moreover, this historical instability was enlarged by the 1854 Ansei Tokai earthquake of *M*w = 8.6. Because of the continuous instability, the downstream river bed is filled with cobbles. These features are common with two more nearby landslides at Shiratori Yama and Ohya (Figure 10). The unstable slope of Shiratori Yama (Figure 12) is made of 'cobbles' (Figure 13) and fell down twice during the 1707 Hoei earthquake of *M*w = 8.7 (Inokuchi and Yagi, 2013) and then the 1854 Ansei Tokai earthquake (Fujii, 1977).

Fig. 9 Map of quoted sites in Japan

The bigger Ohya Landslide (Figure 14) legendarily collapsed during the 1707 Hoei earthquake and, since then, has been unstable for three centuries. The rock at Ohya site is fractured into small pieces (Figure 15) and suggests the past deteriorating effect of tectonic actions of many faults in its vicinity (Figure 16). Furthermore, creep deformation in Ohya is verified by linear depression and the downstream river channel is filled with cobbles.

Although the landslides mentioned above have historical duration, their activities lasted for hundreds or one thousand years only. Hence, their geomorphological effects are not very clear. In contrast when the duration is millions of years or more, different effects of existing fault become clear. One of such examples is the formation of fault valley as a consequence of easy erosion in fractured rock mass. Figure 17 demonstrates such a case of the Median Tectonic Line (MTL) in Central Japan (Figure 9) that is a strike-slip fault and has a long history of 80 million years (Matsushima and Okada, 1993). This long history enabled the erosion process of nature to form a long straight valley. The local geology along this 'Ina' segment of MTL is accompanied by many slope instabilities; see a site of rainfall-induced landslide in Figure 18. Following the past studies in this Ina Valley, Author collected records of affecting earthquakes and flood disasters and plotted their years of occurrence. As the past studies (mentioned in Figure 19) suggested, the periods of high seismicity are followed by the era of heavy rainfall disasters that most likely include sediment disasters. It is supposed, therefore, that the earthquake shaking affected the stability of mountain slopes that had been already deteriorated by accumulation of long-term dislocation along MTL.

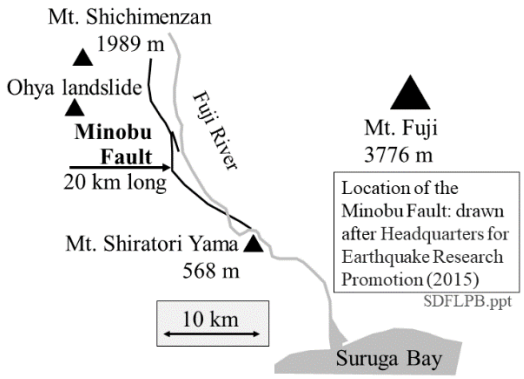

Fig. 10 Location of Minobu Fault, central Japan (drawn after Headquarters for Earthquake Research Promotion, 2015)

Fig. 11 Slope failure of Shichimenzan Mountain

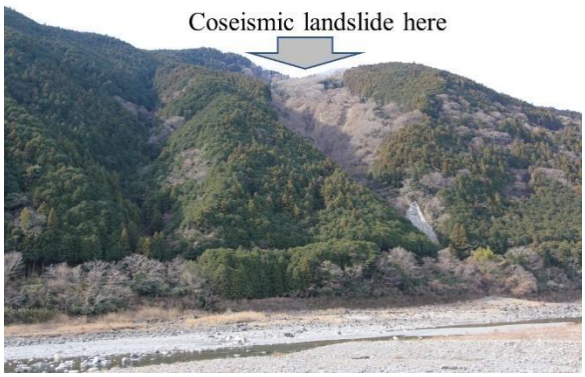

Fig. 12 Shiratoriyama coseismic landslide that failed in 1707 and 1854

Fig. 13 Cobble deposit at the failure site of Shiratoriyama

Fig. 14 Ohya landslide as seen down-ward from its top

Fig. 15 Fractured rock of Ohya landslide site

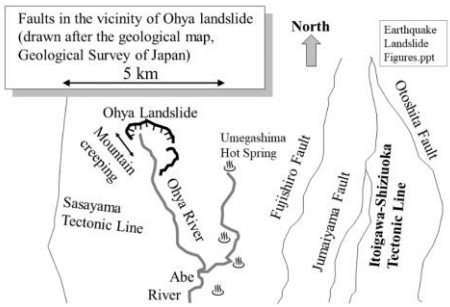

Fig. 16 Location of faults near Ohya landslide site

Fig. 17 Straight fault valley formed along the Median Tectonic Line (Ina Segment) in Central Japan

Fig. 18 Ohnishiyama rainfall-induced slope failure in apparently fractured geology, Ina segment of MTL

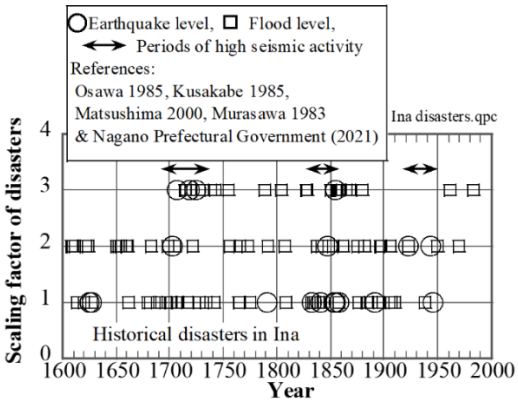

Fig. 19 Possible correlation between intense seismic events and size of flood disasters in Ina

CORRELATION BETWEEN EXISTING FAULT AND THE EXTENT OF EROSION

It is not uncommon that a river flows in a fault valley. In reality, attention is called upon in an opposite way that a fault valley is made by river (erosion). Therefore, dam engineers have to be careful to identify a fault valley thus produced and avoid siting a dam on an active fault. Clyde Dam in New Zealand (Figure 20) and Sigang Dam in Taiwan (Figure 21) were such examples and underwent seismic risk. Accordingly, the former is prepared to accommodate strike-slip dislocation by installing wedges across the concrete dam body, whereas the latter was destroyed by substantial fault dislocation during the 1999 Chi Chi earthquake. The damage in Figure 21 exhibits the power of fault dislocation that can easily destroy a massive concrete structure. Obviously, fault dislocation can produce significant fracturing and disintegration in rock mass.

Fig. 20 Clyde Dam in Southern Island of New Zealand

Fig. 21 Sigang Dam that was destroyed by fault uplift during the 1999 Chi Chi earthquake

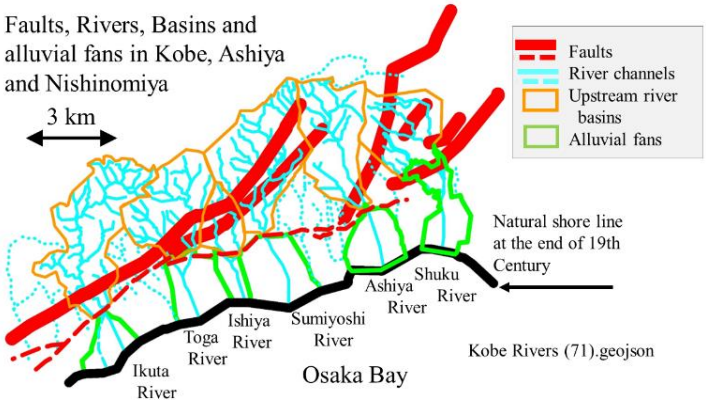

Fig. 22 River basins and alluvial fans to be studied in Kobe (faults and river channels illustrated by broken lines are not considered in the present study)

The following sections address the fracturing and deterioration of mountain slopes as a consequence of prehistoric long-term fault action. Because the fracturing and deterioration result in erosion in the upstream watersheds, this issue can be studied quantitatively by comparing the length of existing faults in mountains and the amount of sedimentary deposits in the downstream areas.

To discuss the effect of fault activities in the upstream area on the rate of erosion and sediment transportation, examples are taken of six rivers in Kobe (Figure 22) that are namely Ikuta River, Toga River, Ishiya River, Sumiyoshi River, Ashiya River and Shuku River from west to east in Figure 22. All of them flow in the southern flank of the Rokko Mountains that started to uplift about one million years ago (Hujita, 1968). It is expected that the size relationship between the upstream basin and the downstream fan may be affected by the existence of faults in the basin. Figure 23 depicts the alluvial fan of the Sumiyoshi River. The six watersheds are situated in the same Rokko Mountains. Therefore, the material or geological properties of the mountains such as mechanical strength and weathering-proneness similarly affected the progress of erosion. Only difference among the watersheds is the effect of fault dislocation.

Fig. 23 Alluvial fan of the Sumiyoshi River

The major difference among six rivers lies in the length and location of active faults in their upstream erosion areas. In the western part of Figure 22, faults are located immediately behind the foot of the mountain slope and most part of the river basin does not have a fault. Furthermore, the faults inside a fan or at the foot of the mountain slope are ignored because they do not affect the erosion in the upstream area. Their influence on the size relationship of erosion areas and alluvial fans is small. In the eastern part, on the contrary, the faults are extended into mountains and have most probably deteriorated the rock mass therein. Noteworthy is that the upstream of Sumiyoshi River is flowing along fault valleys (Maruyama and Lin, 2000). The size of the basin was decided by examining the 1:25,000 map of the GIAJ (Geospatial Information Authority of Japan) surveyed in 1932-1935 which is well prior to artificial modification of land shape in mountains. The size of the fans was determined by referring to the older but less precise 1:20,000 maps of GIAJ surveyed in 1886 where the natural coast lines prior to man-made island construction in 20th Century are illustrated.

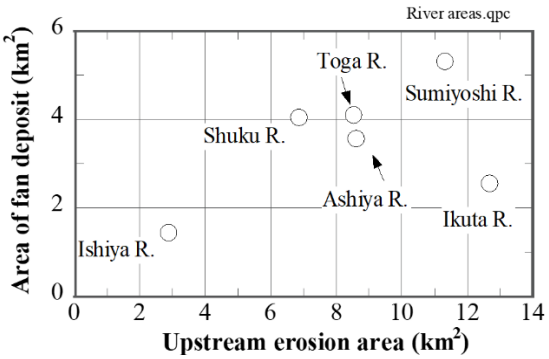

Fig. 24 Relationship between area of upstream river basin and the downstream alluvial fan of rivers (R = 0.51)

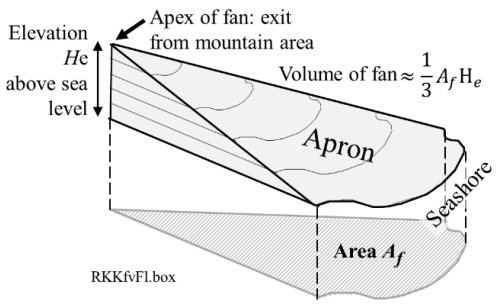

Fig. 25 Model of fan deposit for approximate assessment of its volume

The watersheds and alluvial fans of the six studied rivers were illustrated in Figure 22. Then, their areas are examined in Figure 24 in which a positive correlation is recognized. This suggests that the bigger upstream area of erosion can produce the greater size of the alluvial fans. Although this point is understandable, the correlation coefficients, *R*, is 0.51 which is not satisfactory. The issue is that the product of mountain erosion can be more reasonably evaluated in terms of the sediment volume in place of area.

The volume of the deposit was assessed in an approximate manner as illustrated in Figure 25 in which the area of fan is denoted by A_f and the height of this deposit, *He*, was determined by the elevation of the tip of the fan (or exit of the river stream from mountains), while the elevation of fan perimeter was set at the sea shore (0 m above sea level). Note that the method in Figure 25 ignores the sediment that stays under the present sea level (the sea level used to be higher in warm periods and lower in glacial periods) or flowed into the sea and lost from the fan. The present study assumes that this type of 'error' affects the data of six rivers equally because they are located in very similar geological environment. Hence, no more discussion is made of this 'error'. The results were plotted in Figure 26 and the correlation coefficient for the fan volume decreased to 0.35. Thus, the fan volume does not improve the correlation.

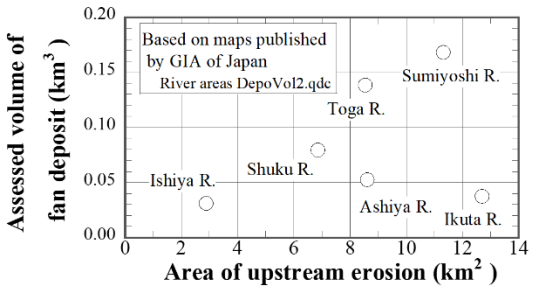

Fig. 26 Relationship between area of upstream river basin and assessed volume of alluvial fan (R = 0.35)

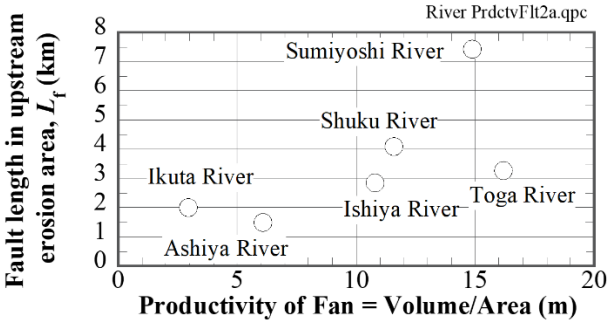

Fig. 27 Correlation between the fan productivity and the fault length in the upstream area (R = 0.68)

To achieve better correlation, the assessed fan volume was divided by the area of the upstream erosion to be called 'productivity'. Figure 27 plots this productivity against the fault length, L_f, in the upstream erosion areas. There is a better correlation here (correlation coefficient = 0.68) to show that the higher fan productivity is associated with the longer fault length, inferring that the rock disturbance by long-term translation of the faults increased the fan productivity or efficiency of erosion in mountains in upstream areas. This is particularly the case of the Sumiyoshi River having the longest fault length.

FINDINGS FROM 2023 TÜRKIYE-SYRIA EARTHQUAKES

The coseismic disaster in February, 2023, in Türkiye (formerly called Turkey) and Syria was caused by a series of earthquakes. The author visited the affected sites in early June, 2023, and studied the spatial distribution of damages including those of slopes and buildings. In the present paper, the attention is focused on the biggest event of *M*w=7.8 that is called the Pazarcık earthquake.

Fig. 28 Building damage in Kahramanmaraş

Heavy damage (Figure 28) was reported, first, in Kahramanmaraş in the central part of Figure 29. Furthermore, the damage was heavy as well in Antakya near the southwestern (SW) end of the fault-parallel coordinate in the figure. The author supposes that the Antakya damage was total devastation, while that in Kahramanmaraş was less devastating. Accordingly, the earthquake motion records over the entire region in Figure 29 were studied to find that the SW parts were hit by motion with stronger amplitude and longer period that appears more destructive to structures there. For publication, the research details were summarized in Towhata et al. (2024).

Figure 30 plots the peak ground acceleration (PGA) at AFAD stations along the fault-parallel coordinate in Figure 29. AFAD is a governmental authority in charge of disaster and emergency management. It is shown here that PGA upper bound increases towards the (south) western end of the fault to which Antakya is close. Note that PGA was strong as well at Pazarcık near -50 km of the fault coordinate. This is most likely because of its short distance to the epicenter but the damage therein was negligible.

To explore the second factor that influenced the damage extent, Figure 31 was prepared in which the velocity response spectra at places of different damage extents are compared. It is found first that the spectra in alluvial sites in Antakya and Kahramanmaraş are characterized by lower-frequency response (<1 *Hz*) whereas, in contrast, the Pazarcık spectrum has peaks at higher frequencies. Moreover, the hilly area of Kahramanmaraş has low response velocity throughout the plotted frequency range. This finding implies that the worst damage extent in Antakya is related with the biggest response values in the low frequency range, and is followed by the damaged alluvium in Kahramanmaraş, while less damaged sites have low response spectra in the low frequency range. Obviously, the alluvium in Kahramanmaraş had more amplification in low frequency range than in its hilly area. The above discussion on frequency and damage is reasonable from the viewpoint of resonance with the natural frequency of houses and buildings. Then a question arises why PGA was strong (Figure 30) and frequency was low (Figure 31) in Antakya.

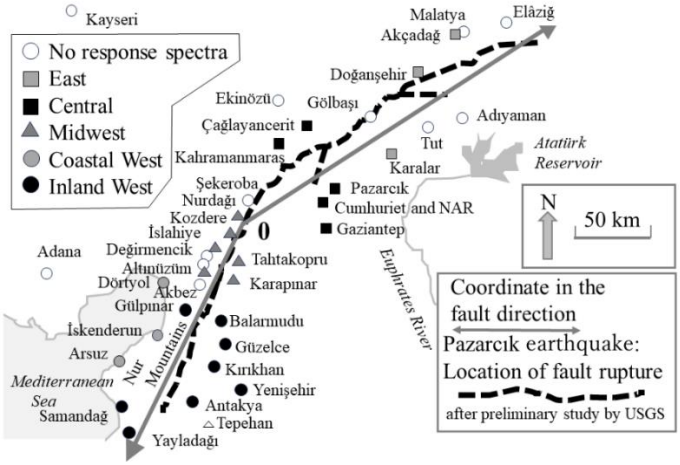

Fig. 29 The affected region in south Türkiye, sites of AFAD earthquake motion recording illustrated by circles, squares, and triangles, and local coordinate set approximately along the causative East Anatolian Fault

Figure 32 plots the arrival time of the main (S-wave) phase of ground motion at places close to the fault coordinate (see Figure 29). The first arrival occurred obviously near the epicenter and then the arrival took place to the east, then followed by the western part. Because the observation points are close to the fault coordinate, it is reasonable that the gradient of coordinate versus time stands approximately for the rupture propagation velocity, V_R, of the fault. The data in this figure suggests that V_R lies between 3 and 5 km/s in most part and particularly in the western segment of the fault. By reasonably assuming that the *S*-wave propagation velocity in earth crust is V_S = 3 km/s, the following discussion is made of the phenomenon of supershear in which $V_R > V_S$.

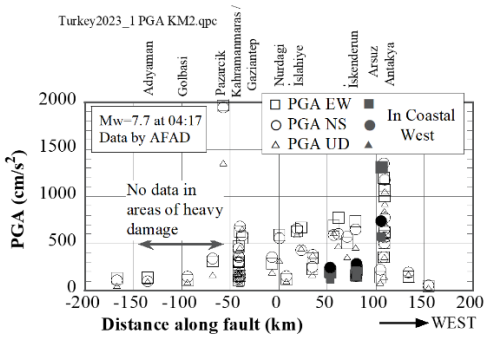

Fig. 30 Distribution of NS and EW peak ground acceleration along the along-fault coordinate

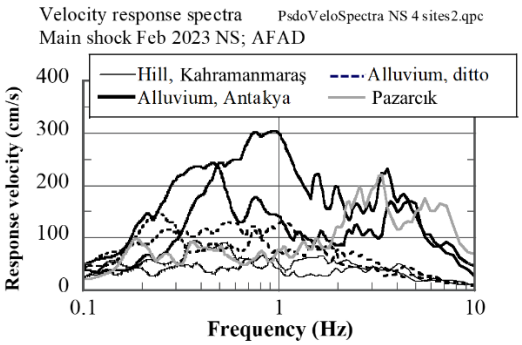

Fig. 31 Comparison of velocity response spectra at severely damaged sites in alluvium of Antakya and Kahramanmaraş against less damaged Kahramanmaraş hills and Pazarcık near the epicenter

Supershear is characterized by the formation of Mach front which is a concentration of wave energy within a small space and time (Figure 33). This kind of rupture occurred presumably during the 1999 Izmit earthquake (Mw = 7.6) (Bao et al., 2022), the 2018 Palu/Sulawesi earthquake of Mw = 7.5 in Indonesia (Socquet et al., 2019) and a few more. Importantly, the 2023 event in Türkiye was associated with detailed ground motion records for the first time. Figure 34 illustrates a simple 2-D model for wave propagation. The causative fault is divided into many (N in number) small segments and the rupture propagates from its left end (x = 0) towards the right end (x = L). The time difference of ruptures between two consecutive segments is $(L/N)/V_R$ and the wave energy propagates in the radial direction.

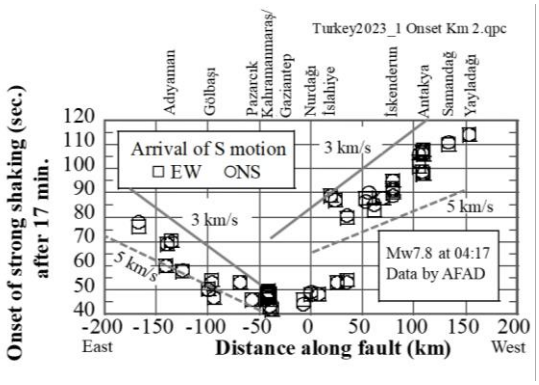

Fig. 32 S-wave arrival time in records at points along the fault coordinate

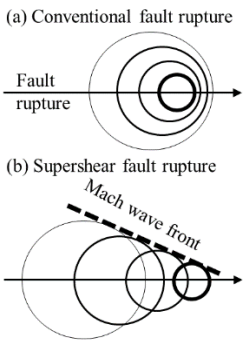

Fig. 33 Comparison of supershear and non-supershear propagation of fault rupture

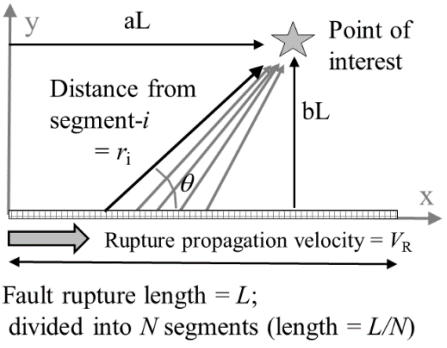

Fig. 34 Conceptual model for numerical calculation of supershear fault rupture and ground response

Figure 35 compares the energy arrival per unit time at points of y=0.1*L. The energy per time is theoretically equivalent with *velocity*^{2}. In case of non-supershear (Figure 35a), the peak energy arrival per unit time is approximately 2 (called normalized non-dimensional energy per time). Then, a supershear was calculated with consideration of the directional energy emission (double-couple mechanism) that is

maximum in *x* and *y* directions while zero in the intermediate directions. The total energy emission was held unchanged from that of the uniform emission. The results in Figure 35b indicates that the intensity of motion was nearly 500 times greater than the case of non-supershear. This difference is equivalent with approximately 20-times difference in velocity. Of further interest is that the maximum energy arrival increases from a = 0.2 towards a = 0.8 near the end of the fault, as observed in Antakya. Although these findings are affected by simplification in modelling, they are still consistent with the field observation.

(a) Non-supershear; V_R/V_S=0.75;
360-degree uniform energy radiation

(b) Supershear; V_R/V_S=1.2;
Energy radiation by double-couple model

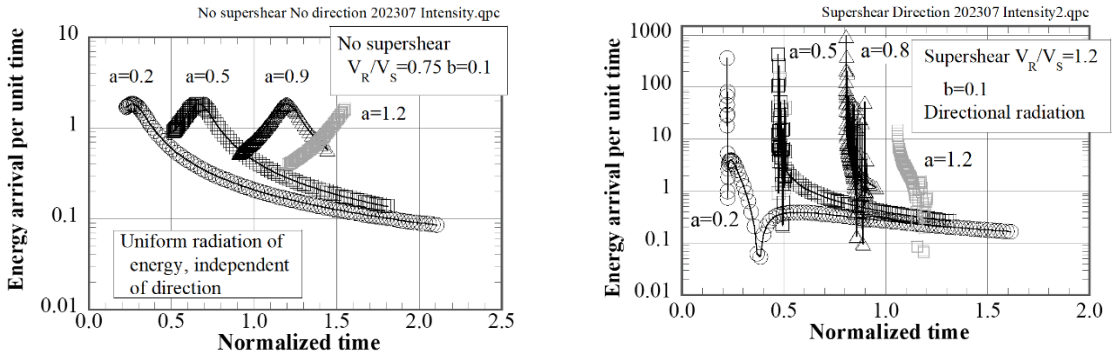

Fig. 35 Energy arrival per time or intensity of velocity response caused by supershear fault rupture (calculated at point of $x=aL$ and $y=bL$ with b = 0.1)

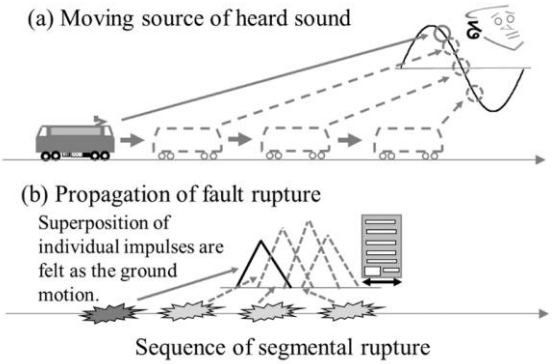

Fig. 36 Conceptual sketch to illustrate the difference between period shortening in Doppler effects and period elongation in supershear earthquakes

The records of earthquake in Türkiye also revealed the lowering of frequency of shaking towards the end point of fault rupture (Figure 31). This issue appears contradictory against the knowledge of Doppler effects. Figure 36 accounts for this point by showing that the signal in Doppler effects is emitted by a single moving source, whereas the observed earthquake motion is a superposition of many short impulses produced by ruptures with short time difference (Figure 33). Figure 37 illustrates such a superposition to demonstrate that the period of the superimposed time history (thick curve) is longer than that of the component impulses. Although still conceptual, this idea explains the reason of low-frequency shaking in Antakya.

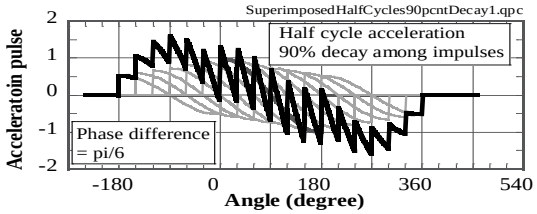

Fig. 37 Proposed idea on mechanism of elongated period or lower frequency of ground motion as a consequence of supershear fault rupture

TECTONIC UPLIFT AS A CONSEQUENCE OF FAULT DISLOCATION

The 2024 Noto Peninsula earthquake of *M*w = 7.5 triggered profound damage not only in buildings and infrastructures but also in mountain slopes and cliffs (Figures 38 and 39). Furthermore, a new negative experience for disaster mitigation discipline was the effect of coseismic uplift along the northern coast of Noto Peninsula (Figure 9). Because the causative fault mechanism off the coast was of a reverse type in which its southern side moved upwards, the coastal area underwent substantial uplift. Figure 40 indicates what happened in Kuroshima Harbor and the uplift was as large as 3 meters. This uplift dried up the harbor and made the access of fishing boats impossible. Figure 41 shows even a worse situation in Kaiso Fishing Harbor where the uplift was 4 m. This is the biggest uplift during this earthquake.

From the viewpoint of geology and geomorphology, coseismic uplift shown above is a natural phenomenon and coastal terraces as seen at many places in the world are the consequences of uplift as well. From social viewpoints, on the contrary, the effect of uplift made a substantial impact on the local community and is still affecting the progress of recovery during the aftermath. The major issues related with uplift are summarized in what follows;

Fig. 38 Coseismic landslide at Ichinose, Noto Peninsula

Fig. 39 Coseismic fall of sea cliff made of tuff, Nagahashi, Noto Peninsula

Fig. 40 3-m uplift of sea bed in fishing harbor of Kuroshima, Noto Peninsula

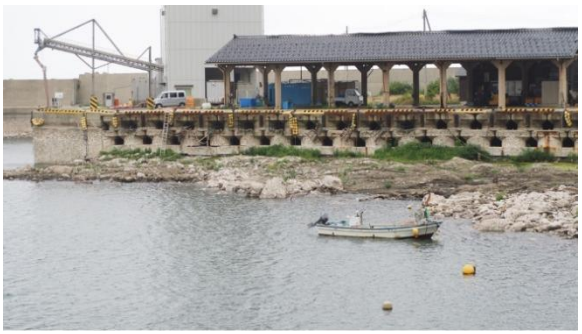

Fig. 41 4-m uplift of fishermen's harbor at Kaiso, Noto Peninsula, where the foundation of quay is exposed

- Wajima City had fire immediately after the earthquake. Because water pipelines were broken, the city firefighters tried to get water from a river. Unfortunately, the land had uplifted 2 meters or so, the river water had gone into the sea and no water was available any more for firefighting. Since there was no way to extinguish the fire, the city center was burnt down completely.
- Rescue materials had to be transported via mountain roads that had undergone landslide problems at many places. Therefore, rescue was slow and very difficult.
- Recovery of seabed uplift (subsidence) was unlikely, although the 1946 Nankai earthquake and the 2011 Tohoku earthquakes were followed by slow recovery in the coseismically dislocated coastal areas.
- One of the major industries in Noto Peninsula is fishing and the uplift of the fishing harbors (Figures 40 and 41) are fatal issues for sustainability of local communities. From the engineering viewpoints, the operation of the harbors can be resumed by digging the uplifted sea bed (as practiced in Muroto Harbor, Japan, after the 1946 Nankai earthquake of *M*w = 8.4; Muroto City Government, 1989) or constructing new harbors at offshore relevant locations. The problem is the needed cost, which

is a difficult issue because the local population and the number of fishermen are decreasing and the expenditure of public funding on this diminishing industry is controversy.

- In particular, the age of the fishermen are 60 years old or more and ageing does not stop.
- Merger and unification of several harbor groups into one may make it possible to allocate public funding on reconstruction of one important fishing harbor and promote quick recovery of the local fishing industry. This is, however, difficult again because geographic expansion (merger) of fishing sea area means that fishermen of other villages come into one's own sea, and catch and sell fish. Local people cannot easily accept this situation.
- In summary, the earthquake in Noto Peninsula indicated that recovery and reconstruction of remote rural areas with decreasing population are not easy because the public financial support for areas without clear future scope is difficult to be approved by financial sectors.
- Consequently, as of August, 2024, the post-seismic efforts for recovery are very slow.

CONCLUSIONS

This paper addressed the recent unsolved topics in earthquake disasters with emphasis on fault actions. First, it was shown that a fault area has rock deterioration due to fault-induced deformation and undergoes slope disasters for a long time. Second, a quantitative study on relationship between faults in the upstream watersheds and the extents of erosion was made of six rivers coming out of Rokko Mountains, Kobe, in order to quantitatively verify the promotion of mountain erosion by the rock deterioration effects of fault dislocation (formation of process zone). Third, supershear of fault rupture was identified with reference to the 2023 earthquake in Türkiye. Fourth, the uplift of ground caused by reverse fault action and induced social problems during a recent earthquake were introduced. Then, last but not least, special appreciation is expressed to AFAD of the Türkiye Government that obtained detailed motion records of supershear earthquake and made them available to the research community.

REFERENCES

1. Bao, H., Xu, L., Meng, L.S., Ampuero, J-P, Gao, L. and Zhang, H.J. (2022). "Global Frequency of Oceanic and Continental Supershear Earthquakes", *Nature Geoscience*, Vol. 15, No. 11, pp. 942-949.
2. Chang, L.C. (1938). "Reconnaissance on Diexi Earthquake in Sichuan Province, Geological Review", *publ. Geological Society of China*, Vol. 3, No. 3, pp. 251-292 (in Chinese).
3. Fujii, T. (1977). "Coseismic Landslide of Shiratori-Yama Mountain triggered by Ansei Tokai Earthquake", *Shizuoka Chigaku*, Vol. 35, No. 33-37 (in Japanese).
4. Hasegawa, S., Dahal, R.K., Yamanaka, M., Bhandary, N.P., Yatabe, R. and Inagaki, H. (2009). "Causes of Large-Scale Landslides in the Lesser Himalaya of Central Nepal", *Environmental Geology*, Vol. 57, No. 6, pp. 1423-1434.
5. Headquarters for Earthquake Research Promotion, (2015). "Long-Term Assessment on Behavior of Minobu Fault", https://www.jishin.go.jp/main/chousa/15apr_chi_kanto/ka_16.pdf as of June 5, 2025 (in Japanese).
6. Hujita, K. (1968). "Rokko Movements and its Appearance – Intersecting Structural Patterns of Southwest Japan and Quaternary Crustal Movements", *The Quaternary Research*, Vol. 7, No. 4, pp. 248-260 (in Japanese).
7. Inokuchi, T. and Yagi, H. (2013). "Shiratori-Yama Landslide Caused by the Hoei Earthquake in 1707". *Journal of the Japanese Landslide Society*, Vol. 50, pp. 147-148 (in Japanese).
8. Kanagawa Prefectural Government, (1986). "Prediction of Seismic Damage in Kanagawa Prefecture", pp. 13-63 (in Japanese).
9. Kingdon-Ward, F. (1955). "Aftermath of the Great Assam Earthquake of 1950", *Geographical Journal*, Vol. 121, pp. 295-303.
10. Kusakabe, A. (1985). "Earthquake in Ina Recorded in Historical Documents", *Ina*, Vol. 33, No. 2, pp. 65-73 (in Japanese).

11. Maruyama, T. and Lin, A. (2000). "Tectonic History of the Rokko Active Fault Zone (Southwest Japan) as Inferred from Cumulative Offsets of Stream Channels and Basement Rocks", *Tectonophysics*, Vol. 323, No. 3-4, pp. 197-216.
12. Matsushima, N. (2000). "Tensyou Earthquakes in the Ina Valley", *Historical Earthquakes*, Vol. 16, pp. 53-58 (in Japanese).
13. Matsushima, N. and Okada, A. (1993). "Active Faults in Ina Tectonic Basin and Median Tectonic Line in Akaishi Mountains", *Document Center for Fault Research* (in Japanese).
14. Meng, W., Xu, Y., Cheng, W.C. and Arulrajah, A. (2018). "Landslide Event on 24 June in Sichuan Province, China", *Preliminary Investigation and Analysis, Geosciences*, Vol. 8, No. 2, pp. 39.
15. Murasawa, T. (1983). "Natural Disasters and Poor Harvests in Ina", *2nd Edition, Kitahara Technical Office* (in Japanese).
16. Muroto City Government, (1989). "History of Muroto City", Vol. 1, pp. 609-611 (in Japanese).
17. Nagai, O. and Nakamura, H. (2000). "The Large-Scale Landslide of Mt. Shichimen - The Study on the History of the Landslide and the Enlargement Process", *Journal of the Japan Landslide Society*, Vol. 37, No. 2, pp. 20-29 (in Japanese).
18. Nagano Prefectural Government, (2021). "List of Damaging Historical Earthquakes, *Appendix 1 for Disaster Mitigation Plan* (in Japanese).
19. Oldham, R.D. (1899). "Report on the Great Earthquake of 12th June, 1897", *Memoir of Geological Survey India*, Vol. XXIX.
20. Osawa, K. (1985). "Toyama Earthquake in Ina", *Ina*, Vol. 23, No. 2, pp. 74-77 (in Japanese).
21. Regmi, A.D., Yoshida, K., Dhital, M.R. and Devkota, K. (2013). "Effect of Rock Weathering, Clay Mineralogy, and Geological Structures in the Formation of Large Landslide, a Case Study from Dumre Besei Landslide, *Lesser Himalaya Nepal*", *Landslides*, Vol. 10, pp. 1-13.
22. Sato, H.P., Hasegawa, H., Fujiwara, H., Tobita, S., Koarai, M., Une. H. and Iwahashi, J. (2007). "Interpretation of Landslide Distribution Triggered by the 2005 Northern Pakistan Earthquake Using SPOT 5 Imagery", *Landslides*, Vol. 4, No. 2, pp. 113-122.
23. Socquet, A., Hollingsworth, J., Pathier, E. and Bouchon, M. (2019). "Evidence of Supershear During the 2018 Magnitude 7.5 Palu Earthquake from Space Geodesy", *Nature Geoscience*, Vol. 12, No. 3, pp. 192-199.
24. Towhata, I., Çağlayan, P.Ö., Tönük, G., Erginağ, U.C. and Torisu, S.S. (2024). "From Reconnaissance on Ground Motion Induced by the 2023 Türkiye-Syria Earthquake", *Journal of Earthquake Engineering*, Vol. 29, No. 5, pp. 981-1022.
25. Vermilye, J.M. and Scholz, C.H. (1998). "The Process Zone: a Microstructural View of Fault Growth", *Journal of Geophysical Research*, Vol. 103, No. B6, pp.12223-12237.
26. Zhou, Q. and Chen, X.C. (2012). "Asymmetrical Disaster Distribution and its Cause Analysis of the Mw7.9 Wenchuan Earthquake", *15th WCEE Lisbon*, Vol. 3, pp. 1626-1635.
27. Zhou, Q., Zhang, C.S. and Chen, X.C. (2011). "Asymmetric Disaster Distribution and its Cause Analysis of the Ms8.0 Wenchuan Earthquake", *Acta Seismologica Sinica*, Vol. 33, No. 4, pp. 492-504 (in Chinese).